THE JOURNAL OF PHYSICAL CHEMISTRY C

Article

Hydrolytic Stages of Titania Nanoparticles Formation Jointly Studied by SAXS, DLS and TEM

Alexey Tarasov, Verena Goertz, Eugene Alexeevich Goodilin, and Hermann Nirschl

J. Phys. Chem. C, **Just Accepted Manuscript** • DOI: 10.1021/jp312443u • Publication Date (Web): 20 May 2013

Hydrolytic Stages of Titania Nanoparticles Formation Jointly Studied by SAXS, DLS and TEM

Alexey Tarasov[&,ξ,*] , Verena Goertz[ξ], Eugene Goodilin[&], Hermann Nirschl[ξ]

& – Faculty of Materials Science, Lomonosov Moscow State University; Lenin Hills, 119992, Russia

ξ - Institute of Mechanical Process Engineering and Mechanics, Karlsruhe Institute of Technology (KIT), Campus Sued, Straße am Forum 8, 76131, Germany

Author Information

Corresponding author

* Laboratory of Solid State Ionics, Institute of Problems of Chemical Physics RAS, Academician Semenov avenue 1, Chernogolovka, Moscow region, 142432 Russian Federation; E-mail: alexey.bor.tarasov@gmail.com

Abstract

A thermohydrolysis of titanium compounds solutions is a widely used method for titania-based nanomaterials preparation. The relationship between properties and synthetic conditions of such materials is derived from the nature of processes occurring in solution during the material formation. In the present paper, new insights on titania nanoparticles formation by thermohydrolysis of $TiCl_4$ water solution are given based on a joint study by SAXS, DLS and TEM techniques. The key stage was supposed to rely on a bonding rearrangement process inside an inorganic polymer causing a crystalline phase formation characterized by 3-4 nm gyration radii according to SAXS. The model of $TiCl_4$ thermohydrolysis describing the whole process of the TiO_2 nanoparticles formation was supposed. The presence of several

distinct steps allows one to control phase composition and morphology of the final nanoparticles of titania opening up the possibility to vary their functional properties.

Keywords

Nanomaterials, TiO_2, TiCl4, thermohydrolysis, Small-Angle X-Ray Scattering

Introduction

Nowadays titania seems to be one of the most industrially demanded materials widely used as a white pigment, photocatalyst for water and air purification, photosplitting and a semiconductor for solar cells[1,2,3,4]. Titania crystalline structure, morphology and size are known to be crucial for its practical applications. Therefore formation mechanism studies and new preparation methods development become drastically important[5]. Among the known approaches of TiO_2-based material preparation, hydrolysis of different titanium derivatives like titanium complexes, halogenides or alkoxides compounds allows to obtain unique materials with various morphologies and phase compositions predetermining demanded physical characteristics. Nearly single-sized titania microspheres with a given mean diameter could be synthesized via hydrolysis of titanium alkoxides in different organic solvents[6,7], hydrothermal treatment of $TiCl_3$ water solution in the presence of $FeCl_2$[8] or aging tetrabutyl titanate in an ethylene glycol-acetone mixture. Also a uniform rodlike rutile TiO_2 nanocrystals[9], mesoporous titania spheres with chamber-like structure[10], nanocrystalline TiO_2 powders[11], monodispersed titania microspheres, composed of densely packed radially aligned rutile nanorods[12] were synthesized via Ti-derivatives hydrolysis under different preparation conditions.

Titanium tetrachloride remains the most important Ti precursor for TiO_2 production by gas-phase oxidation[13] or liquid-phase hydrolysis[14,15,16,17,18,19,20,21]. At the same time, a few possible hydrolysis mechanisms were suggested only on the ground of

correlation between products properties and preparative routes[20,21,22,23], computer simulation[24] and by using dynamic light scattering (DLS) and transmission electron microscopy (TEM) [25] or small angle X-ray scattering (SAXS)[26].

In this article we present an in-depth investigation of major stages of thermohydrolysis of acid aqueous $TiCl_4$ solutions by a combined study of small angle X-ray scattering (SAXS), dynamic light scattering (DLS) and transmission electron microscopy (TEM) techniques, assisted by the pH-measurements *in situ*. The results demonstrate several new features and suggest a possible mechanism for formation of titanium dioxide that can help to understand the difference in morphology and functional properties of related materials depending on synthesis route.

Theory

The X-ray scattering intensity was experimentally determined as a function of the scattering vector q whose modulus is given by $q = \left(\frac{4\pi}{\lambda}\right)\sin(\frac{\varphi}{2})$, where λ is the wavelength of the incident radiation and φ is the scattering angle.

The scattering intensity I(q) of aggregates is defined by

$$I(q) = \frac{N_p}{V_p I_o(0)} P(q) S(q) \quad (1)$$

where N_p and V_p are number of particles and particle volume, respectively[27,28]. P(q) is the form - factor normalized by $I_0(0)$

$$P(q) = I(q) / I_o(0). \quad (2)$$

The structure factor S(q) describes the interactions between particles. Typical structure factors for fractal aggregates with a mass fractal dimension D^{mf} can be

estimated as $S(q) \sim (qR_G)^{-Dmf}$, where R_G is the radius of gyration[28]. The mass fractal dimension D^{mf}, the primary particles' radius of gyration R_G and the particle surface are the most important characteristics of agglomerates.

The scattering curves of aggregates in a dual logarithmic scale consist of three linear segments. The first one is the Guinier regime omitted for our camera due to the limited scattering vector range. Two experimentally detected linear segments are the Power law and the Porod law regime intersecting in a transition point. The slope in the Power Law segment has been related to the mass fractal dimension of the aggregate D^{mf} [28]. For the second observed linear segment the slope, P, in the Porod Law region has been related to the surface fractal dimension D^{sf}: $P = 6-D^{sf}$ [29]. The position of the transition between the Power and Porod Law regimes reflects the mean particle size: the radius of gyration of primary particles can be estimated from the transition point using the Guinier relation[30]:

$$I(q) = I(0)\exp(-\frac{q^2 R_G^{\ 2}}{3}) \quad (3)$$

Experimental

$TiCl_4$ solutions were prepared by dropwise addition of pure $TiCl_4$ (Fluka, >99.0%, (AT)) to a hydrochloric acid (0.6 mol/**L**) at ~0°C under constant stirring. The final $[Ti^{4+}]$ concentration in the prepared solution was about 0.3 mol/**L**. A solution with [Ti] = 0.012 mol/**L** was prepared by diluting the concentrated acidic $TiCl_4$ solution with distilled water.

Thermohydrolysis was performed in a 500 mL three-neck-flask at two different temperatures, 80°C and 90°C. Reaction was carried out under reflux condition and air atmosphere. The solution was heated in a water bath under constant stirring for six hours. The measurement of the reaction time was started when the flask was

immersed into the water bath. The temperature and pH values of the hydrolyzing solution were measured by a pH-meter (pH/Cond 340i, WTW GmbH, Germany) using a glass electrode equipped with a thermocouple. After the beginning of thermohydrolysis, 5 mL volume samples were taken by a pipette within a time period between 5 and 300 min. The samples were placed in 10 mL glass vials and quickly cooled down to ambient temperature under running water.

To perform an XRD analysis, the solution obtained after thermohydrolysis was sprayed into liquid nitrogen and then freeze-dried in aluminium pan at p=0.15 mbar and T_{sh}=-30÷20^{o}C for 48 h. Sample powders were examined using Rigaku D/MAX 2500 (Japan) with a rotating copper anode (CuK_{α} irradiation, 5 – 90^{o} 2θ range, 0.02^{o} step). Diffraction maxima were indexed using the PDF-2 database.

Dynamic Light Scattering experiments were performed with a Zetasizer Nano ZS (Malvern Instruments) setup equipped with a helium-neon laser (λ = 632.8 nm, 4 mW power) and a thermoelectric temperature controller. Measurements were taken at the 90° scattering angle in a 3×3-mm quartz cuvette. Each sample was measured three times and the particle size (hydrodynamic diameter) was averaged.

SAXS experiments were conducted with a modified Kratky camera in the range of 0.1 ≤ q ≤ 1.2 nm^{-1}. The camera was equipped with a copper anode (X-ray tube KFL Cu, line focus 0.4 × 12 mm, Siemens, X-ray generator Kristalloflex 760 Bruker AXS), a Göbel mirror, a slit collimator and an image plate detector. Due to the finite dimension of the primary beam, the scattering data had to be slit length and slit width desmeared. The samples were placed in a quartz capillary of 1 mm diameter and wall thickness of < 30 μm. The software IgorPro version 4.00 (WaveMetrics, Lake Oswego, OR, USA) containing the Irena 1 SAS macro was used for the evaluation of the radius of gyration and the slopes of the different scattering regimes.

TEM images were acquired using a Philips CM 12 microscope operating at 120 kV. For these measurements, carbon-coated grids were briefly dipped into the sample and dried under atmospheric pressure.

Results

The final phase composition of the obtained nanoparticles was investigated by XRD (Figure 1) using the powder originated from freeze-dried solution. All the peaks were found to correspond to anatase (A) except some impurity of aluminum chloride hexahydrate (*) ([21-1272] and [73-301] cards of PDF-2 data base, respectively), formed occasionally from the material of aluminium pan. This conventional finding is the result of multiple stages of transformation of the system under thermal hydrolysis conditions as described below.

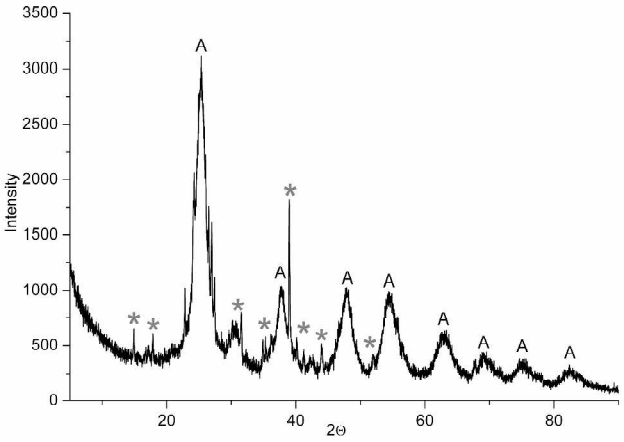

Fig. 1

The hydrolysis of $TiCl_4$ has been monitored through the measurement of solution pH values during the process. In Figure 2 the temperature dependence of the solution pH is shown for two experiments performed at 80°C and 90°C. In both the cases the pH value remains approximately constant (~1.4) until the temperature reaches ~52°C. From that time the pH value starts to decrease gradually due to subsequent heating.

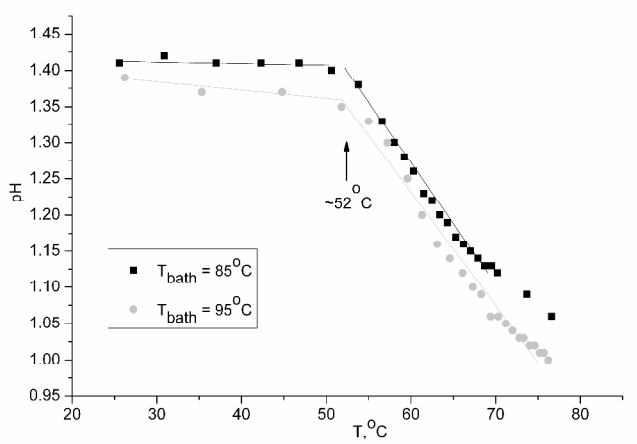

Fig. 2

The DLS measurements data (Figure 3) show the same qualitative behavior of the particle diameters at 80 and 90°C e.a. the diameter increases almost linearly during the first hour up to its maximal value and then it decreases gradually in time.

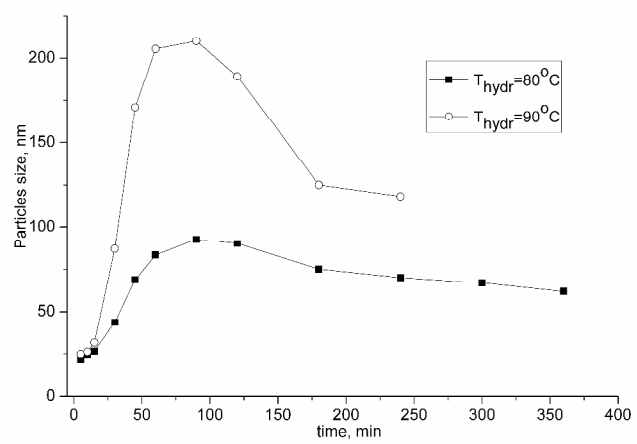

Fig. 3

TEM images of the samples taken after different reaction time at 90°C are shown in Figure 4. The nature of the intermediate products is not *a priori* known and thus morphology evolution would be associated, first of all, to composition changes. In these terms, different characteristic morphologies of the particles observed by TEM are characteristic of the steps of final crystalline phase formation. After 5 min of thermohydrolysis, TEM image shows unshaped structures which amount increases in the 10 minutes sample. Elongated structures with a net-like morphology appear in the

samples taken after 15 min. After 60 minutes, particle aggregates are seen for the first time. The sample taken after 180 minutes shows aggregates of well-shaped nanoparticles of about 10 nm in size.

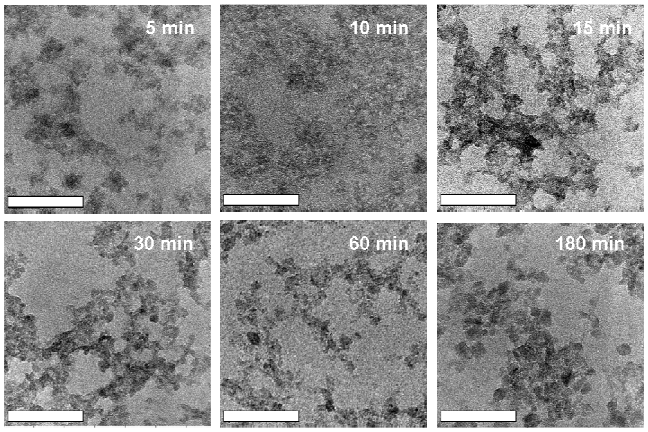

Fig. 4

The scattering curves of the samples taken at different time of thermohydrolysis are plotted in Figure 5a and 5b. Figure 5a shows the scattering curves measured after 5 min (squares), 10 min (circles) and 15 min (triangles). The scattering curve measured after 5 min has one well-shaped transition point at q=0.3 nm^{-1}. The intensity of the scattering curve after 10 min is higher than the intensity measured after 5 min in the whole q-vector range and has already two transition points (see inset in Figure 5a). The first transition point can be found at a smaller scattering vector q = 0.27 nm^{-1} than the curve measured after 5 min of thermohydrolysis. The scattering curve after 15 min has also two transitional points. The intensity of the scattering curve is the same as after 10 min. The first transitional point is placed at the scattering vector q = 0.25 nm^{-1}. The second transition point is more noticeable and is located at the same q-vector as after 10 minutes. Scattering curves from the samples collected after 30, 45, 60, 120, 180 and 240 minutes are shown in Figure 5b. The curves have an offset of y = 0.15. After 240 min the scattering curves don't change anymore. Due to the limitation of the scattering vector range, only the second

transitional point can be seen in Figure 5b. The mass fractal dimensions D^{mf} of the aggregates and the surface fractal dimensions D^{sf} of the primary particles in dependence on the reaction time are plotted in Figure 5c and 5d. The radii of gyration for the second transitional points were estimated with Guinier exponentional equation (chapter 3) and are plotted in Figure 6.

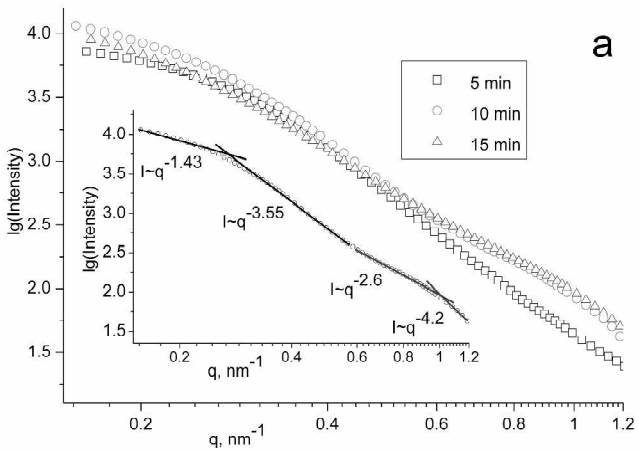

Fig.5a

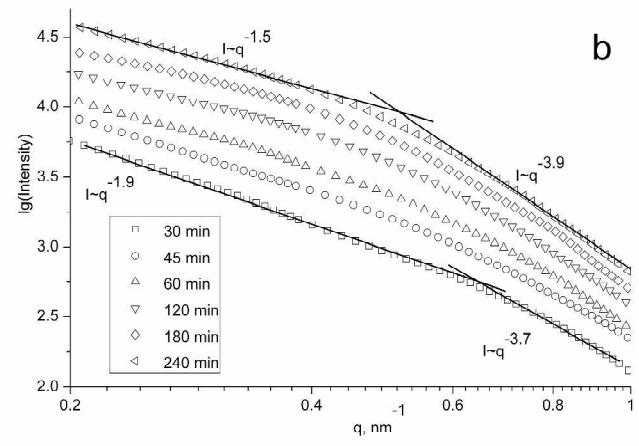

Fig. 5b

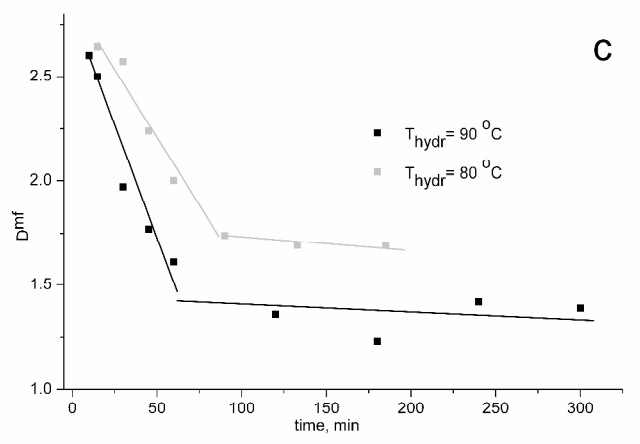

Fig. 5c

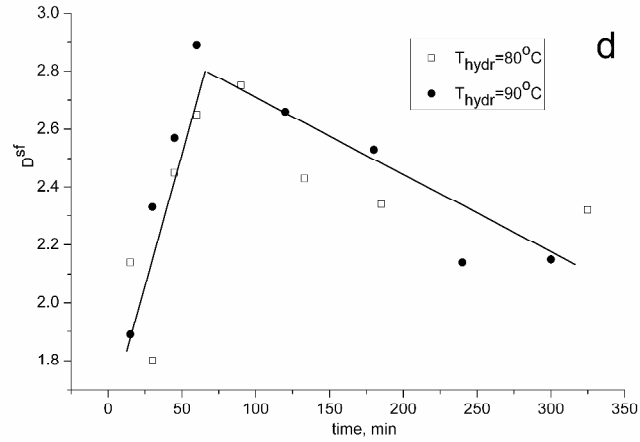

Fig. 5d

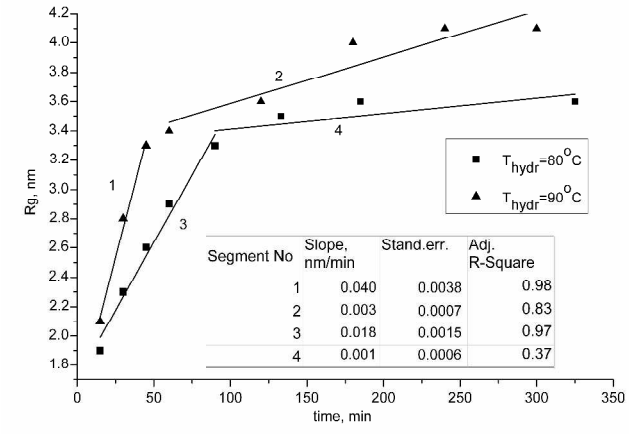

Fig. 6

Discussion

The anatase formation under the applied preparation conditions (low $TiCl_4$ concentration and relatively high pH) agrees with the Pottier's scheme[20]. $TiCl_4$ exists in acid aqueous solutions at ambient temperature and low concentration as octahedral hydroxochlorocomplexes like $[Ti(OH)_aCl_b(OH_2)_c]^{(4-a-b)+}$ where a + b + c = 6, as shown elsewhere[31]. The values a and b depend on the acidity and the concentration of Cl^- in the solution[31]. Consequently, it is very plausible that the thermohydrolysis of the complex $[Ti(OH)_aCl_b(OH_2)_{6-a-b}]^{(4-a-b)+}$ could lead to a progressive increase of hydroxylation ratio OH/Ti, from a=1 up to a=4-b (a value corresponding to the non-electrically charged complex), and Cl^- ligands exchange with OH^-. Thus the formed octahedral hydroxyl-aqua complex molecules react through olation and oxolation processes and form titanium dioxide[20]. Accordingly, a decrease of the solution pH value observed in the beginning of the thermohydrolysis is expected during the first stage of process. In our case, the decrease of the pH value at ~50°C would mean that the complex $[Ti(OH)_aCl_b(OH_2)_{6-a-b}]^{(4-a-b)+}$ becomes unstable after a certain critical temperature of the solution and Cl^- ligands exchange with OH^- of water which leads to octahedral hydroxyl-aqua complex formation and to pH decreasing.

In order to investigate the features of solid matter formed from titanium octahedral hydroxyl-aqua complex, DLS measurements were performed to determine the hydrodynamic diameter of the particles in solution as described above (Figure 3). Such behavior might be explained by a change of particle internal structure during the hydrolysis namely the density of the particles aggregates should vary. Unfortunately the DLS technique provides information only about an average (overestimated) hydrodynamic diameter of the particles and gives no information about its internal features. TEM and SAXS were used to clarify the details.

The evolution of the particles structure during the process of 90°C - thermohydrolysis can be divided into two different stages. The first stage is characterized by the formation of nanoparticles with a gyration radius of 6.5 nm in SAXS and hydrodynamic diameter 25 nm in DLS. The difference in particle sizes expressed as the hydrodynamic diameter from DLS and the diameter calculated from radius of gyration obtained by SAXS should be attributed to the distinction between these two parameters in application to particle aggregates such as porous unshaped bodies. In agreement with TEM data, these nanoparticles were interpreted as clots of inorganic polymer, generated in solution by thermohydrolysis of the complex $[Ti(OH)_aCl_b(OH_2)_{6-a-b}]^{(4-a-b)+}$. As stated before, the scattering intensity obtained after 10 minutes is higher than that after 5 minutes. This was attributed to an increase of the total amount of scattering centers in solution and polymeric clots. After 10 minutes of reaction the clot radius of gyration determined by SAXS reaches 7 nm. The hydrodynamic diameter in the DLS measurements gives 26 nm. The intensity of the scattering curve obtained after 15 minutes is the same than the one after 10 min. The clot radius of gyration determined from the first transitional point is increased up to 7.5 nm. The second transitional point of this curve could be attributed to the pores filled with water inside the inorganic polymer. In these terms, the first stage of the process seems to take place between 3 and 10 minutes and can be shortly defined as “inorganic polymer” formation.

In the sample taken after 30 min the clot size is too large for the available q-vector range but remains detectable by the DLS technique. The hydrodynamic diameter of the particles in solution measured with DLS increased up to 87 nm (Figure 3). The shape of the scattering curve seems to be typical for nanoparticle aggregates. This might be explained by the transformation of the inorganic clots into aggregates of the primary nanoparticles. The mass fractal dimension D^{mf} changes significantly between

10 and 60 minutes. After 10 minutes of the synthesis D^{mf} is ~2.6, which means porous solid "particles" while after 60 minutes it is already ~1.6 for 90°C synthesis and ~2 for 80°C and corresponds to the aggregates of the particles. At the same time the surface fractal dimension of the primary particles D^{sf} increases up to ~2.8 which characterizes a very rough diffusion surface. The gyration radius of the primary particles increases with the rate ~ 0.04 nm/min and 0.018 nm/min for 90°C and 80°C syntheses respectively. Such a behavior can be explained either by the changing in the solid matter's density or by the disintegration of the already formed aggregates.

After 60 minutes the trend drastically changes since the surface fractal dimension of the primary particles D^{sf} decreases down to 2.2 while the mass fractal dimension D^{mf} remains approximately constant. The growth rate of the primary particles becomes slower, ~0.003 nm/min for 90°C synthesis and ~0.001 nm/min for 80°C. This could be attributed to the smoothing the primary particles surface within already formed aggregates probably due to their faceting.

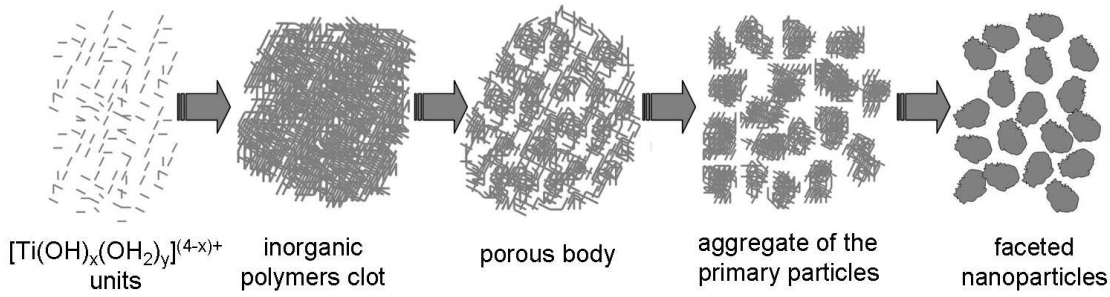

Fig. 7

All the above mentioned findings are summarized in the following possible mechanism of the process shown in Figure 7. By achieving the critical temperature, the complex $[Ti(OH)_aCl_b(OH_2)_{6-a-b}]^{(4-a-b)+}$ becomes unstable and Cl^- ligands exchange with OH^-, which leads to octahedral hydroxyl-aqua complex formation. This stage is characterized by the changing of the pH value of the reaction solution. The formed

$[Ti(OH)_x(OH_2)_y]$ units start to be interlinked by OH groups via the olation reaction and create large inorganic polymers clots detectable by the DLS technique. At a high temperature, the oxolation starts and nuclei of an ordered, crystalline, phase appear and grow inside the inorganic clots. The appearance of the crystalline nuclei is clearly seen by TEM and defines the character of SAXS curves. Water released in the condensation reaction accumulates in the pores inside the inorganic polymer and forms a porous matter. After certain time, initial necks between the particles collapse and aggregates of small primary particles form. This can be clearly seen by the decrease of D^{mf}. A higher temperature of the thermohydrolysis influences the extent of inorganic polymers disintegration and leads to the formation of more branched aggregates with a lower D^{mf} value. Upon the high temperature the particles crystallize and become faceted. Thus the processes of nucleation and growth of titania as a final, well – defined crystalline phase are of complex nature being associated with consequent transformation of inorganic polymers clots and assemblage of an ordered crystalline phase in the course of chemical transformation of the precursors. As a consequence, such composition evolution is likely to be associated with the observed morphological evolution.

The model of $TiCl_4$ thermohydrolysis supposed in the present paper describes the whole process of the TiO_2 nanoparticles formation. In the articles[22,32] some parts of this process were studied separately, nevertheless the whole process wasn't clarified so far. In particular, an interpretation of DLS measurements for initial stages of the process is given by Zhang et al[25]. They have found the formation and growth of nanoparticles in solution during the heating and interpreted them in terms of a homogeneous nucleation theory. However the final stages of the process as well as changes of the internal structure of the nanoparticles during the reaction have not been investigated and discussed properly, because of DLS technique limitations. At

the same time, our DLS measurements are in a good agreement with the data from Zhang's group for final stages of the hydrolysis. SAXS technique is one of the most powerful methods for an investigation of condensed and solid matter as well as for the processes in colloidal systems[32,33,34,35,36,37]. Jalava et al. have studied using SAXS the long-time aging and aggregation of titania colloidal nanoparticles at elevated temperature in terms of mass and surface fractal aggregates formation and these data are also not contradicting with our results. Thus, our data are in good agreement with the published results and it makes us to believe that thermohydrolysis of homogeneous $TiCl_4$ aqueous solution is a powerful tool to reach desired morphology and properties of titania nanoparticles in the frame of the model described above.

Conclusions

Titania nanoparticles formation during thermohydrolysis of $TiCl_4$ water solution was studied with SAXS technique and supported by TEM, DLS and pH-value measurements. The formation of TiO_2 nanoparticles were supposed to go through the bonding rearrangement process inside the inorganic Ti-based polymer toward a crystalline phase formation and the process is divided in several distinct steps.

Acknowledgments

The program of KIT-MSU collaboration *„ZO IV – Understanding and application of complex systems“* and particularly Prof. Dr. Fritz H. Frimmel and Prof. Dr. Irina V. Perminova are acknowledged for financial support. We also thank Dr. Volkov V.V. from the Institute of Crystallography of the Russian Academy of Sciences for his fruitful discussions concerned with an interpretation of SAXS data.

References

(1) Fujishima, A.; Hashimoto, K.; Watanabe, T.; *TiO2 Photocatalysis: Fundamentals and Applications*; Bkc, Tokyo, **1999**.

(2) Fujishima, A.; Honda, K.; Electrochemical Photolysis of Water at a Semiconductor Electrode; *Nature **1972**, 238*, 37-38.

(3) Serpone, N.; Dondi, D.; Albini, A.; Inorganic and Organic UV Filters: Their Role and Efficacy in Sunscreens and Suncare Products; *Inorg. Chim. Ac.* **2007**, *360*, 794-802.

(4) O'Regan, B.; Grätzel, M.; Low-cost, High-Efficiency Solar Cell Based on Dye-Sensitized Colloidal TiO2 Films; *Nature* **1991**, *353*, 737-740.

(5) Bickley, R.I.; Gonzalez-Carreno, T.; Lees, J.S.; Palmisano, L.; Tilley, R.J.D.; A Structural Investigation of Titanium Dioxide Photocatalysts; *J. Solid State Chem.* **1991**, *92*, 178-190.

(6) Fegley, B.; Barringer, E.; Owen, H.K.; Synthesis and Characterization of Monosized Doped TiO2 Powders; *J. Amer. Ceram. Soc.* **1984**, *67*, 113-116.

(7) Eiden-Assmann, S.; Widoniak, J.; Maret, G.; Synthesis and Characterization of Porous and Nonporous Monodisperse Colloidal TiO2 Particles; *Chem. Mater.* **2004**, *16*, 6-11.

(8) Han, Y.; Li, G.; Zhang, Z.; Synthesis and Optical Properties of Rutile TiO2 Microspheres Composed of Radially Aligned Nanorods; *J. Cryst. Growth* **2006**, *295*, 50-53.

(9) Zhang, S.; Liu, C.-Y.; Liu, Y.; Zhang, Z.-Y.; Mao, L.-J.; Room Temperature Synthesis of Nearly Monodisperse Rodlike Rutile TiO2 Nanocrystals; *Mat. Lett.* **2009**, *63*, 127-129.

(10) Li, H.; Bian, Z.; Zhu, J.; Zhang, D.; Li, G.; Huo, Y.; Li, H.; Lu, Y.; Mesoporous Titania Spheres with Tunable Chamber Structure and Enhanced Photocatalytic Activity; *J. Am. Chem. Soc.* **2007**, *129*, 8406-8407.

(11) Kolen'ko, Y.V.; Burukhin, A.A.; Churagulov, B.R.; Oleynikov, N.N.; Synthesis of Nanocrystalline TiO2 Powders From Aqueous TiOSO4 Solutions Under Hydrothermal Conditions; *Mat.Lett.* **2003**, *57 (5-6)*, 1124-1129.

(12) Luo, J.; Gao, L.; Large-Scale Production of Monodispersed Titania Microspheres by Surfactant-Guided Self-Assembly; *J Alloy Comp.* **2009**, *487*, 763-767.

(13) Deberry, J.C.; Robinson, M.; Pomponi, M.D.; Beach, A.J.; Xiong, Y.; Akhtar, K.; Controlled Vapor Phase Oxidation of Titanium Tetrachloride to Manufacture Titanium Dioxide; *U.S. Patent 6,387,347*, May 14, 2002.

(14) Shan, G.B.; Demopoulos, G.P.; The Synthesis of Aqueous-Dispersible Anatase TiO2 Nanoplatelets; *Nanotechnology* **2010**, *21*, 025604.

(15) Fang, C.-S.; Chen, Y.-W.; Preparation of Titania Particles by Thermal Hydrolysis of TiCl4 in N-propanol Solution; *Mat. Chem. and Phys.* **2003**, *78*, 739-745.

(16) Park, H.K.; Kim, D.K.; Kim, C.H.; Effect of Solvent on Titania Particle Formation and Morphology in Thermal Hydrolysis of TiCl4; *J. Am. Ceram. Soc.* **1997**, *80 (3)*, 743-749.

(17) Lee, B.I.; Wang, X.Y.; Bhave, R.; Hu, M.; Synthesis of Brookite TiO2 Nanoparticles by Ambient Condition Sol Process; *Mat. Lett.* **2006**, *60*, 1179-1183.

(18) Garnweitner, G.; Grote, C.; In Situ Investigation of Molecular Kinetics and Particle Formation of Water-Dispersible Titania Nanocrystals; *Chem. Phys.* **2009**, *11*, 3767-3774.

(19) Cassaignon, S.; Koelsch, M.; Jolivet, J.P.; Selective Synthesis of Brookite, Anatase and Rutile Nanoparticles: Thermolysis of TiCl4 in Aqueous Nitric Acid; *J. Mater. Sci.* **2007**, *42*, 6689-6695.

(20) Pottier, A.; Chaneac, C.; Tronc, E.; Mazerolles, L.; Jolivet, J.-P.; Synthesis of Brookite TiO2 Nanoparticles by Thermolysis of TiCl4 in Strongly Acidic Aqueous Media; *J. Mater. Chem.* **2001**, *11*, 1116-1121.

(21) Paola, A.D.; Cufalo, G.; Addamo, M.; Bellardita, M.; Campostrini, R.; Ischia, M.; Ceccato, R.; Palmisano, L.; Photocatalytic Activity of Nanocrystalline TiO2 (Brookite, Rutile and Brookite-Based) Powders Prepared by Thermohydrolysis of TiCl4 in Aqueous Chloride Solutions; *Colloids Surf. A-Physicochem. Eng. Asp* **2008**, *317*, 366-376.

(22) Kinsinger, N.M.; Wong, A.; Li, D.; Villalobos, F.; Kisailus, D.*; Nucleation and Crystal Growth of Nanocrystalline Anatase and Rutile Phase TiO2 from a Water-Soluble Precursor; Cryst. Growth Des.* **2010**, *10(12)*, 5254-5261.

(23) Stötzel, J.; Lützenkirchen-Hecht, D.; Frahm, R.; Santilli, C.V.; Pulcinelli, S.H.; Kaminski, R.; Fonda, E.; Villain, F.; Briois, V.; QEXAFS and UV/Vis Simultaneous Monitoring of the TiO2-Nanoparticles Formation by Hydrolytic Sol-Gel Route; *J. Phys. Chem. C* **2010**, *114 (14)*, 6228-6236.

(24) Wang, T.-H.; Navarrete-Lopez, A.M.; Li, S.; Dixon, D.A.; Gole, J.L.; Hydrolysis of TiCl4: Initial Steps in the Production of TiO2; *J. Phys. Chem. A* **2010**, *114*, 7561-7570.

(25) Zhang, G.; Roy, B.K.; Allard, L.F.; Cho, J.; Titanium Oxide Nanoparticles Precipitated from Low-Temperature Aqueous Solutions: I. Nucleation, Growth, and Aggregation; *J. Am. Ceram. Soc.* **2008,** *91(12)*, 3875-3882.

(26) Hummera, D.R.; Heaney, P.J.; Post J.E.; In Situ Observations of Particle Size Evolution During the Hydrothermal Crystallization of TiO2: A Time-resolved Synchrotron SAXS and WAXS Study; J. Cryst. Growth 2012, 344, 51–58

(27) Wengeler, R.; Wolf, F.; Dingenouts, N.; Nirschl, H.; Characterizing Dispersion and Fragmentation of Fractal, Pyrogenic Silica Nanoagglomerates by Small-Angle X-ray Scattering; *Langmuir* **2007**, *23*, 4148-4154.

(28) Sorensen, C.M.; Light Scattering by Fractal Aggregates: A Review; *Aerosol. Sci. Technol.* **2001**, *35*, 648-687.

(29) Porod, G.; Die Rontgenkleinwinkelstreuung von Dichtgepackten Kolloiden Systemen; *Kolloid Z.* 1951, *124*, 83.

(30) Guinier, A.; *Ann. Phys.* **1939**, *12*, 161.

(31) Nabivanets, B.I.;Kudritskaya, L.N.; A study of the Polymerisation of Titanium(IV) in Hydrochloric Acid Solutions; *Russ. J. Inorg. Chem.* **1967**, *12*, 616-620.

(32) Jalava, J.-P.; Hiltunen, E.; Kahkonen, E.; Erkkila, H.; Harma, H.; Taavitsainen, V.-M.; Structural Investigation of Hydrous Titanium Dioxide Precipitates and Their Formation by Small-Angle X-ray Scattering; *Ind. Eng. Chem. Res.* **2000**, *39*, 349-361.

(33) Kallala, M.; Sanchez, C.; Cabane, B.; Structures of Inorganic Polymers in Sol-gel Processes Based on Titanium Oxide; *Phys. Rev. E*, **1993**, *48(5)*, 3692-3704.

(34) Golubko, N.V.; Yanovskaya, M.I.; Romm, I.P.; Ozerin, A.N.; Hydrolysis of Titanium Alkoxides: Thermochemical, Electron Microscopy, Saxs Studies; *J. Sol-Gel Sci. and Tech.* **2001**, *20*, 245-262.

(35) Boissiere, C.; Grosso, D.; Amenitsch, H.; Gibaud, A.; Coupé, A.; Baccilea, N.; Sanchez, C.; First In-Situ SAXS Studies of the Mesostructuration of Spherical Silica and Titania Particles During Spray-Drying Process; *Chem. Commun.* **2003**, 2798-2799.

(36) Luca, V.; Bertram, W.K.; Sizgek, G.D.; Yang, B.; Cookson, D.; Delineating the First Few Seconds of Supramolecular Self-Assembly of Mesostructured Titanium Oxide Thin Films Through Time-Resolved Small Angle X-ray Scattering; *Langm.* **2008**, *24*, 10737-10745.

(37) Lebon, S.; Marignan, J.; Appell J.; Titania Gels: Aggregation and Gelation Kinetics; *J. Non-Cryst. Solids* **1992**, *147–148*, 92–96.

Figures captures

Figure 1. XRD patterns of the powder obtained after the freeze drying of final solution (90^0C hydrolysis temperature).

Figure 2. pH data versus reaction temperatures measured for 20 minute periods of time in the course of two experiments conducted under different temperatures of a water bath.

Figure 3. The hydrodynamic radius of the particles in reaction solution during the syntheses at different temperatures, measured by DLS technique.

Figure 4. TEM images of the samples taken after different reaction time at 90^0C. Scale bar is 50 nm.

Figure 5. SAXS data for samples obtained at different times during thermohydrolysis process. a,b) scattering curves for different time samples of the 90oC synthesis. Inset in 5a shows the two transitional areas at the scattering curve taken after 10 minutes; c) mass fractal dimension Dmf in dependence on the reaction time and d) surface fractal dimension Dsf for primary particles in dependence on the reaction time for 80oC and 90oC syntheses, calculated as 6-P, where P is the slope of the Porod regime.

Figure 6. Primary particles radius of gyration estimated from SAXS data depending on the reaction time.

Figure 7. A possible mechanism of TiO2·xH2O nanoparticles formation during the thermohydrolysis.

TOC Graphic

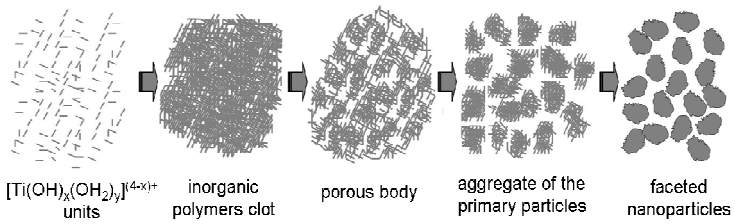
$[Ti(OH)_x(OH_2)_y]^{(4-x)+}$ units
inorganic polymers clot
porous body
aggregate of the primary particles
faceted nanoparticles

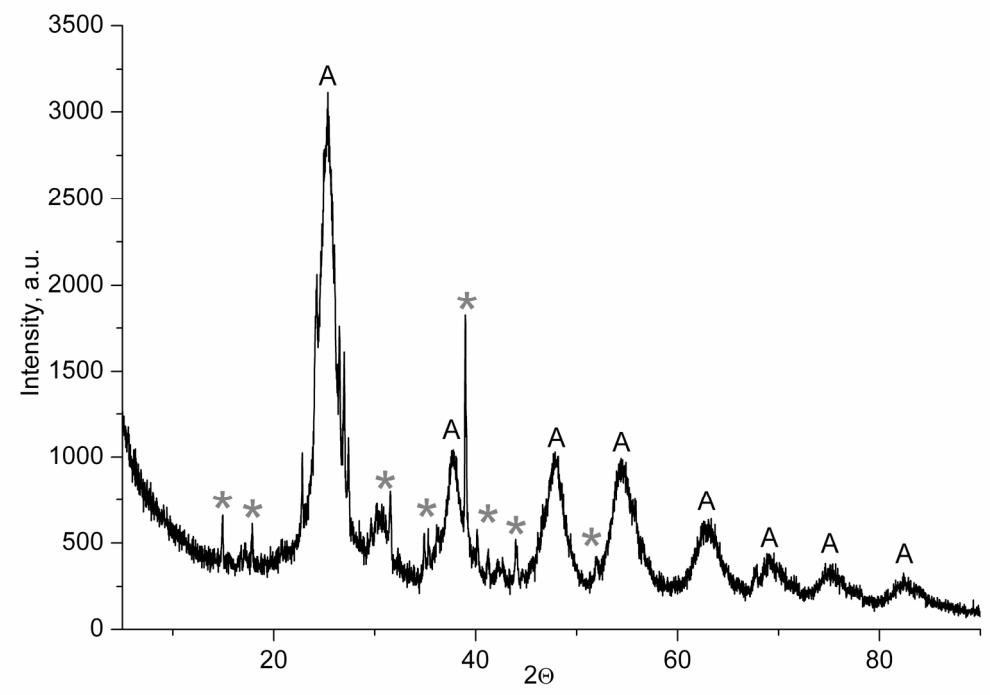

201x140mm (300 x 300 DPI)

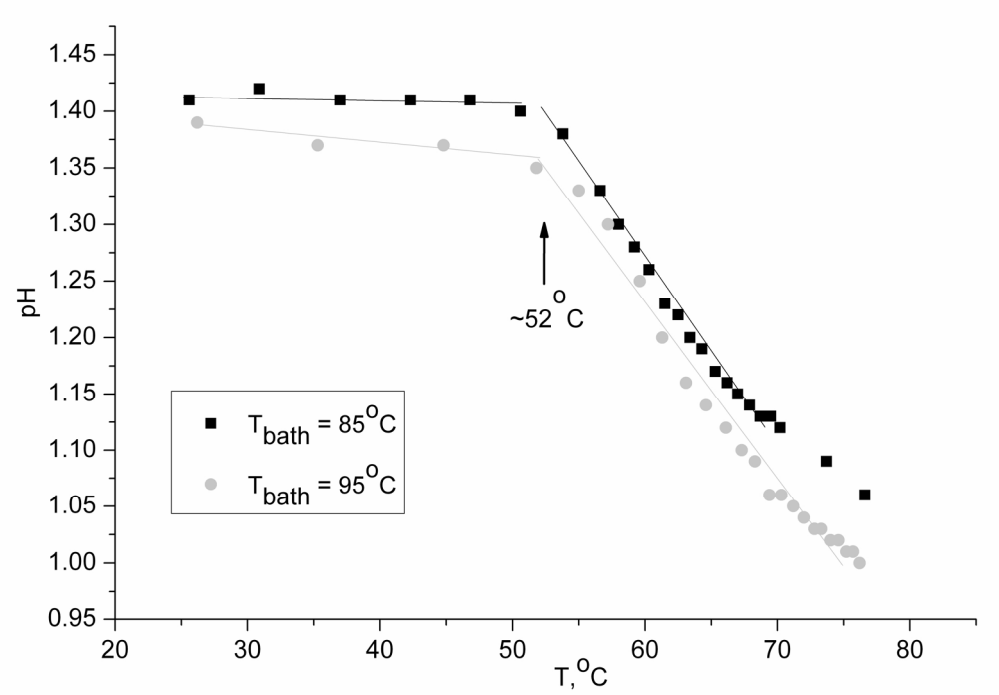

201x140mm (300 x 300 DPI)

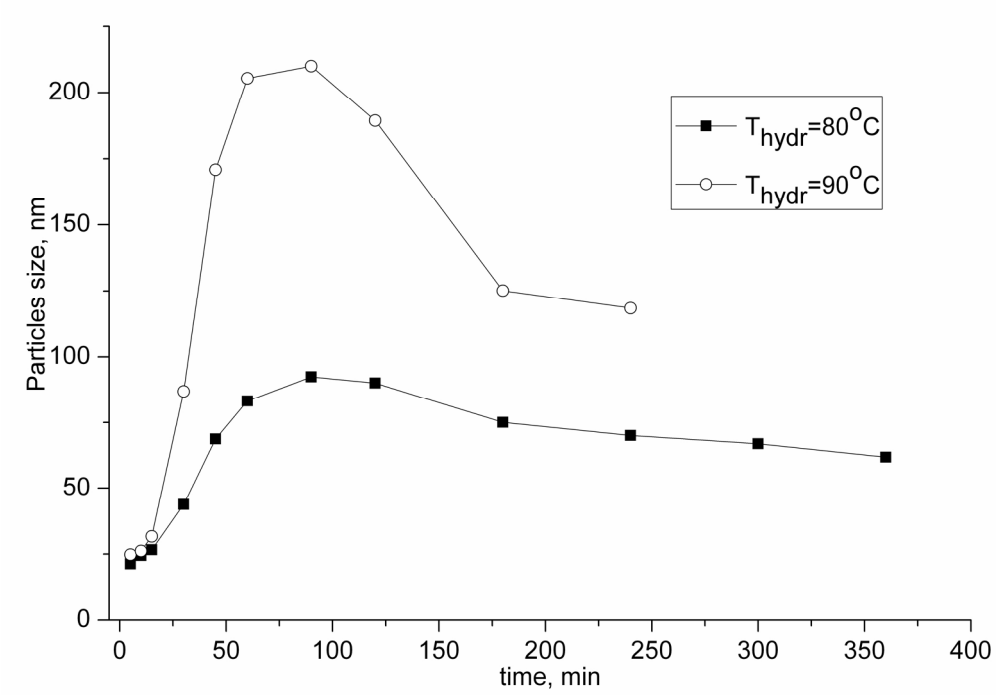

201x140mm (300 x 300 DPI)

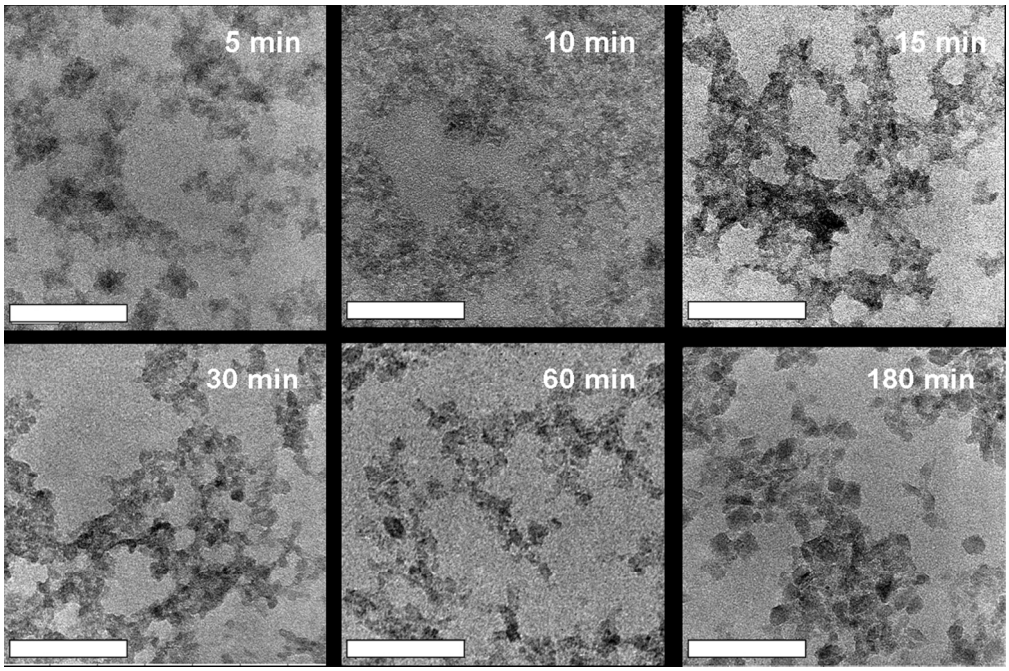

217x143mm (150 x 150 DPI)

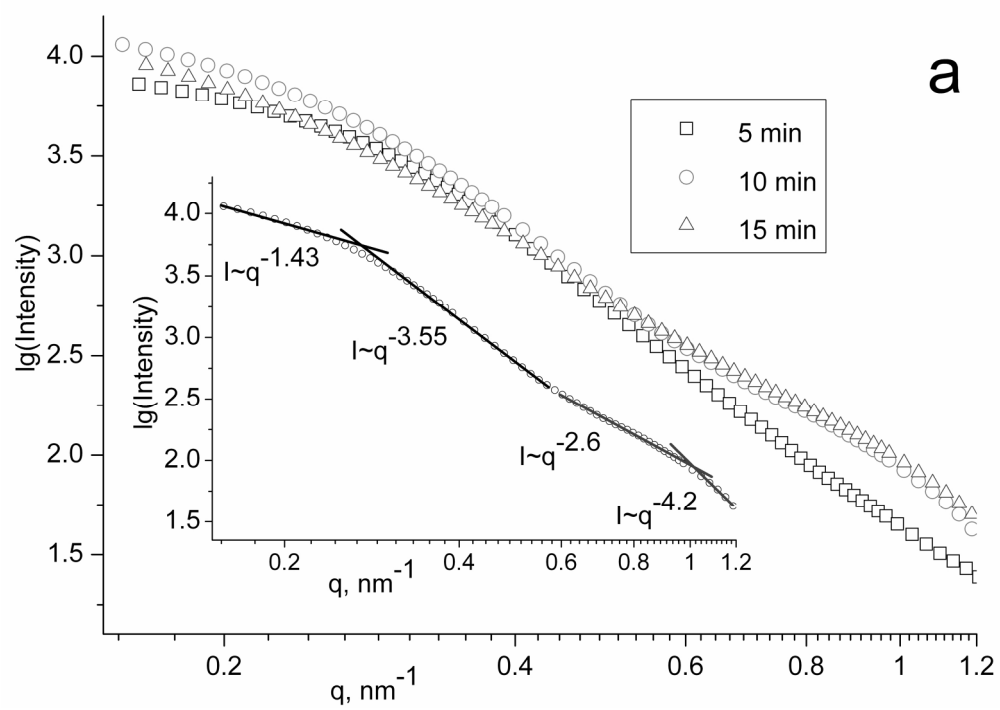

209x148mm (300 x 300 DPI)

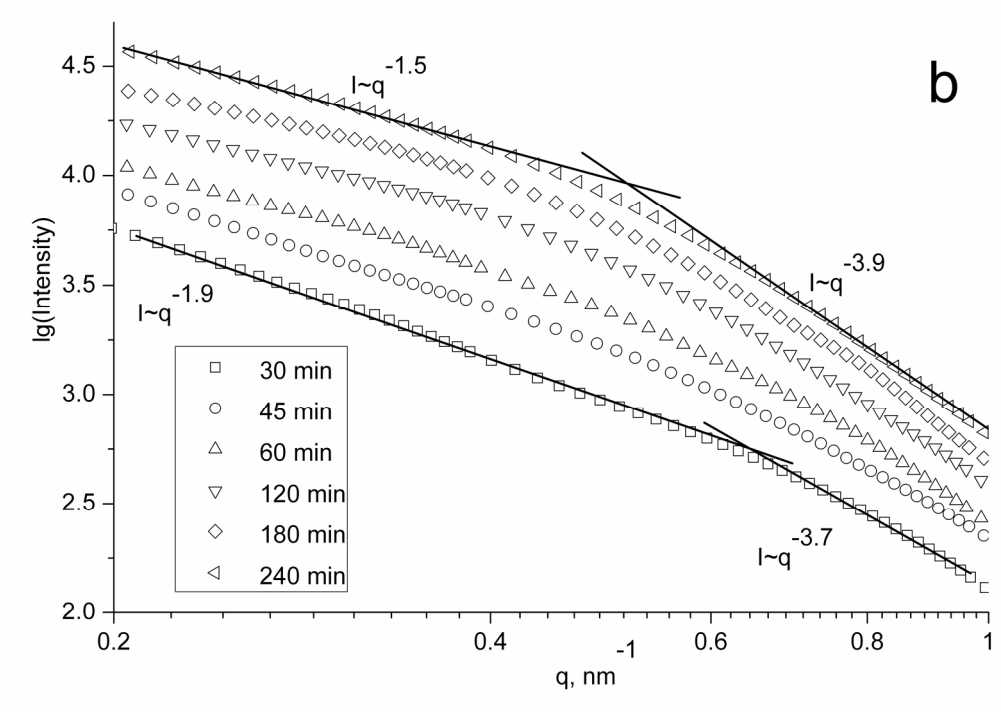

209x148mm (300 x 300 DPI)

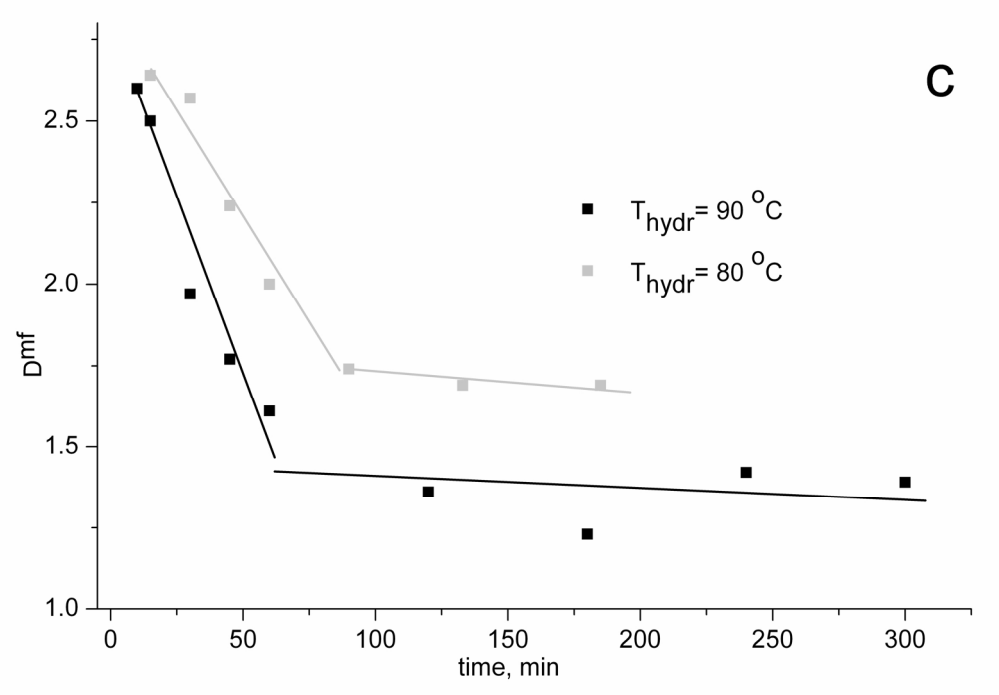

201x140mm (300 x 300 DPI)

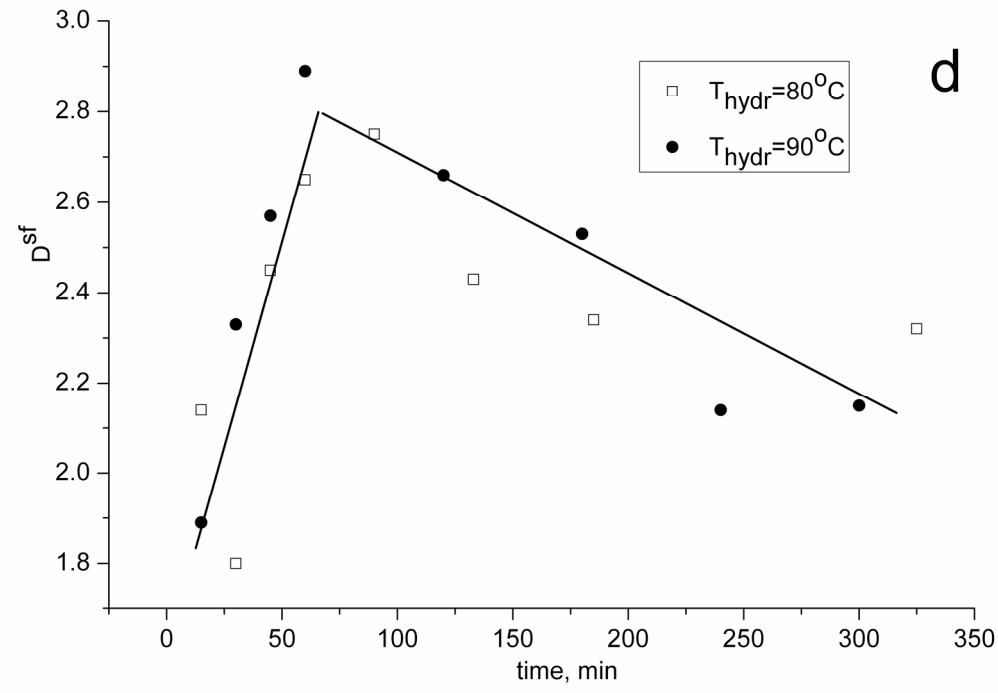

201x140mm (300 x 300 DPI)

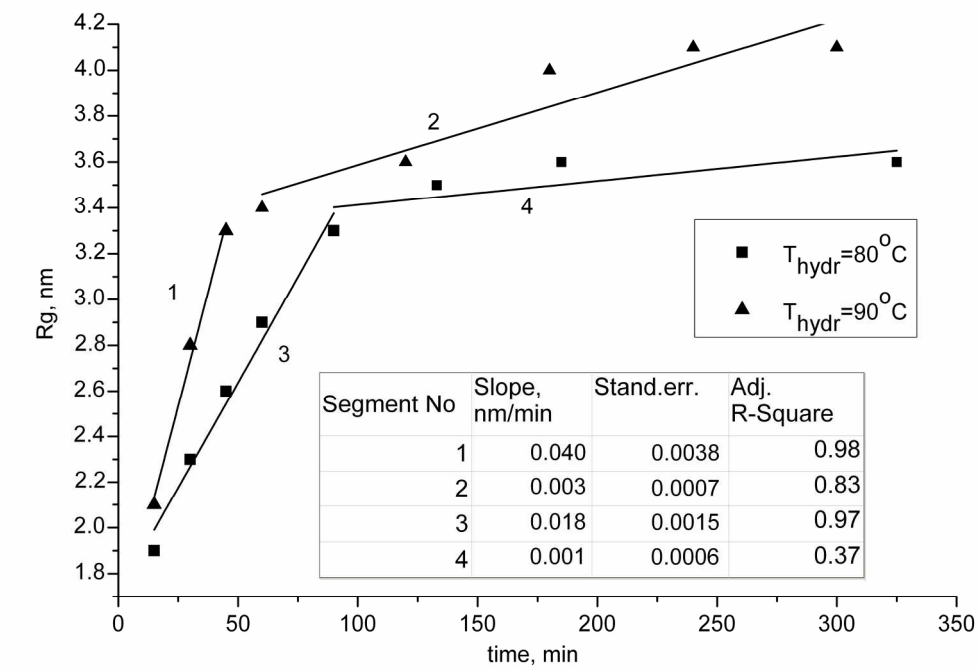

201x140mm (300 x 300 DPI)

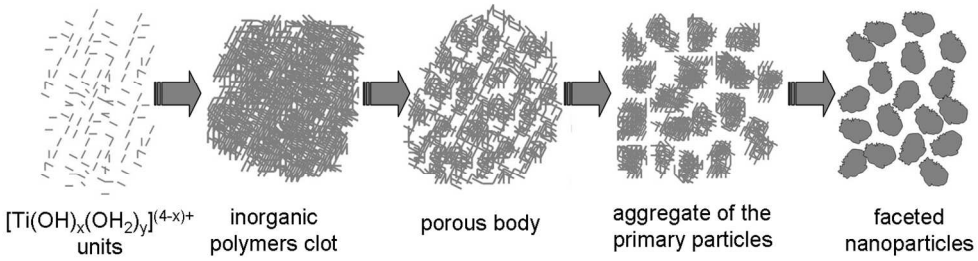

259x70mm (150 x 150 DPI)

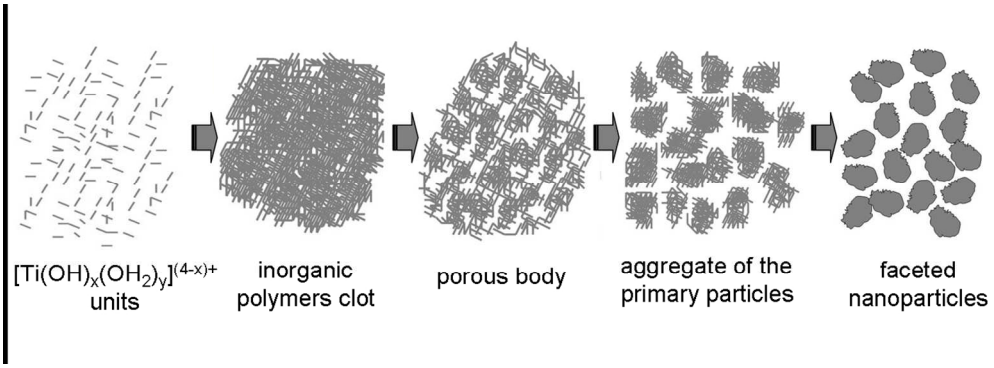

239x86mm (150 x 150 DPI)